Characterizing LEO Objects using Simultaneous Multi-Color Optical Array

Tanner S. Campbell

Department of Aerospace and Mechanical Engineering, University of Arizona, 1130 N Mountain Ave, Tucson, AZ 85721

Prof. Vishnu Reddy

Lunar and Planetary Laboratory, University of Arizona, 1629 E University Blvd, Tucson, AZ 85721

Prof. Roberto Furfaro

Department of Systems and Industrial Engineering, University of Arizona, 1127 E James E. Rogers Way, Tucson, AZ 85721

Scott Tucker

Starizona, 5757 N. Oracle Rd., Tucson, AZ 85704

ABSTRACT

Our goal is to characterize resident space objects (RSOs) in low-Earth (200-1,800 km) and medium-Earth (1,800-35,000 km) orbit using an optical array that collects simultaneous multi-color data. To this effect we have constructed a Multi-Color Optical Array (MOA) telescope on an alt-alt mount capable of tracking RSOs at various altitudes. The primary aperture is 203 mm with an F/1.9 focal ratio. The detector field of view is 2.4 x 1.8 degrees with a pixel scale of 1.8 arc-seconds/pixel. Each RSO has unique spectral characteristics primarily indicative of the material it is made of, however it is also dependent on object attitude, rotation rate, and solar phase angle. These parameters, coupled with the relatively fast motion of objects in LEO and MEO make spectral characterization quite challenging. As such, simultaneous multi-color photometry is the best way to characterize unresolved RSOs, offering multiple independent channels of data that can be used to identify their unique spectral signatures and estimate attitude/attitude rates. Complimentary to this effort we are creating an inventory of common man-made materials found in space so that we may build a spectral database to compare against. With this database, we hope to identify diagnostic absorption bands of common space materials to help aid in our selection of appropriate filters for our optical array telescope and ultimately characterize the RSOs in question.

1. INTRODUCTION

One of the more challenging problems in the field of Space Situational Awareness is object identification. Purely tracking the dynamics of a Resident Space Object (RSO) is not sufficient to "maintain custody" of an object without nearly 24/365 persistent surveillance as some of these objects maneuver. Multi-color photometry can help uniquely identify an RSO in a multi object field of view by providing another dimension of information beyond optical astrometry. In order to accomplish this, a large baseline dataset needs to be established that would catalog the photometric behavior of RSOs to account for observing geometries, orbital regimes, surface composition, and shapes. To this effect, we would like to present results of observing RSOs in different orbital regimes simultaneously with multiple photometric filters. As we develop techniques we hope to show that observing RSOs in multiple wavelengths will enable us to uniquely fingerprint and identify these objects.

2. HARDWARE

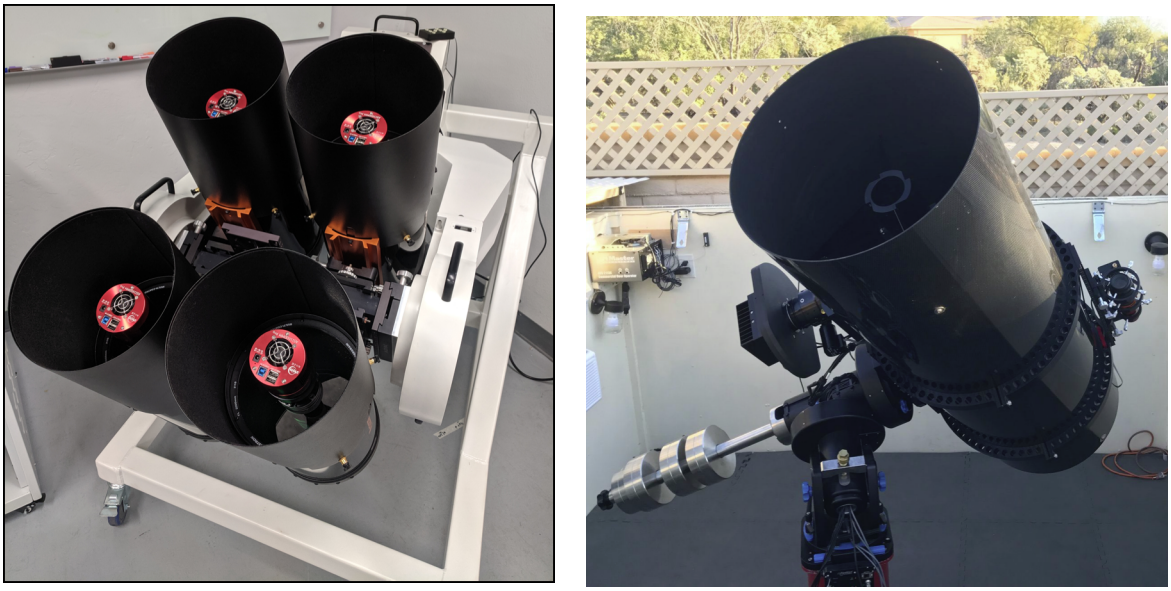

(a) (b)

Fig. 1 Multi-Color Optical Array (MOA) on alt-alt mount (Left) and Leo-20 telescope (Right) .

The data used for this research was collected with two optical sensor systems. As can be seen from Fig. 1a and 1b, the MOA telescope consists of four individual 203 mm Schmidt-Cassegrain telescopes on an alt-alt mount, and the other is 508 mm Leo-20 Newtonian telescope on an equatorial mount. Their basic characteristics can be found in Table 1. The Finger Lakes Instrumentation (FLI) PL4710 on the 508 mm telescope is a back illuminated deep depletion 1K monochrome CCD sensor with 13 μm pixels that has a peak QE of over 90% at 800 nm [7]. The four ZWO ASI 1600MM cameras on the Multi-Color Optical Array (MOA) telescope are 4K x 3K monochrome CMOS sensors with 3.8 μm pixels that have a peak QE of over 60% at 525 nm [8].

Table 1. Telescope and camera parameters that were used to collect data for algorithm and method testing.

Name	Aperture (m)	Focal Length (m)	Camera	FOV (deg)	Pixel Scale (as/px)
MOA	4 x 0.203	0.386	4 x ASI 1600 MM Pro	2.4 x 1.8	1.8
Leo-20	0.521	1.523	FLI ProLine 4710	0.5x0.5	1.76

We have collected data both unfiltered and with Sloan photometric filters listed in Table 2.

Table 2. Bandpass for our photometric filters.

Name	Wavelength (nm)
u’	320-385
g'	401-550
r'	562-695
i'	695-844
z'	>820

3. DATA COLLECTION

While we experiment with different collection methods and algorithms, each of the four cameras on the MOA is controlled independently. As such, a given exposure sequence must be started manually on each camera. This simple approach allows for data to be collected while a more elegant solution is developed. The physical telescope mount is driven by Sidereal Technology software, and images were captured with Maxim DL.

Since we are mainly concerned with photometric measurements in this experiment, we do not need very precise absolute time, and it is only the relative time during an observation sequence that is important. To this effect, we use an ntp web-server to synchronize time across all cameras every minute to keep the clocks from drifting a significant amount.

In order to best capture the rapid dynamics of a LEO satellite transit, very short exposures are required. We selected these cameras in particular due to their high frame rate which allows us to take over twenty frames per second in full resolution, or almost 200 per second if we sub-frame the images. In addition to short exposure times, rate tracking the satellites allows us to maximize the amount of data we can collect on a single pass. To avoid star streaks and maintain good centroids on all objects in the image frames we use Eq. (1) to approximate our ideal exposure time. For most LEO satellites, this yields an exposure time of approximately 0.01 seconds with the MOA. In addition, this exposure time represents under sampling in the Nyquist sense of point sources in the images, and should therefore be doubled. We also elected to use 3 pixel binning along both axes of our sensors which will increase our optimal exposure time calculation. Taking into account our binning and Nyquist sampling, we can now theoretically go up to an exposure time of 0.06 seconds without any impact on our centroid quality. We found, however, that with 3 pixel binning an exposure time of 0.02 seconds was long enough to satisfy Nyquist sampling criteria and see RSOs in LEO and it gives us margin to increase the exposure time to capture fainter objects.

$$t_E = \frac{p_x h}{f' v_s} \tag{1}$$

In Eq. (1) p_x is the size of a detector pixel, h is the altitude of the object's orbit above the observation station, f' is the focal length of the telescope, and v_s is the object's orbital speed. Since Eq. (1) does not consider the number of photons absorbed by the detector in that time, it is quite possible that the time t_E is too short for a "sufficient" detection, and is a purely geometrical relationship.

4. DATA REDUCTION

Our astrometric reduction process is designed for a UNIX-based operating system so that it can be easily scaled for distributed use on High Performance Computing (HPC) systems for rapid analysis of large datasets [1]. To this effect it has been deployed on the CyVerse/VerSSA cyberinfrastructure system at the University of Arizona. To ensure support of a wide array of observations from diverse locations, our reduction pipeline is capable of matching stars with 24 different star catalogs including the recently released massive GAIA DR 2 catalog [10], [11]. Star and object centroids are computed using an iterated isophotal first-order moment with second-order correction given in Eq. (2). The iteration is initialized with a simple isophotal first-order moment, ${}^{(0)}\bar{x}_i$, and follows the scheme:

$${}^{(k+1)}\bar{x}_i = {}^{(k)}\bar{x}_i + 2\frac{\sum_j {}^{(k,j)}w^{(j)}I({}^{(j)}x_i - {}^{(k)}\bar{x}_i)}{\sum_j {}^{(k,j)}w^{(j)}I} \tag{2}$$

Where $i \in \{1,2\}$ denotes the axis of the centroid coordinate (i.e. 'x' or 'y'), k is the iteration index, and j is the summation index over all pixels that belong to a given image object. The ${}^{(j)}I$ are the pixel values and the ${}^{(k,j)}w$ are given by:

$${}^{(k,j)}w = \exp\left(-\frac{{}^{(k,j)}r^2}{2\sigma^2}\right) \tag{3}$$

In Eq. (3), ${}^{(k,j)}r$ is just the Euclidean distance between each pixel in the object and the previous centroid location, and σ is the diameter that contains half of the object flux in the image divided by $\sqrt{8ln2}$. The centroid position is iterated until the change between iterations is less than two ten-thousandths of a pixel (approximately 3 iterations).

This method is chosen because it is more accurate than a simple isophotal centroid, and faster than Point Spread Function (PSF) fitting with very similar accuracy (close to the limit of image noise). Once the pixel locations of the centroid of all light sources in the image are extracted, their relative spacing is cross-correlated with that of stars from the desired catalog. This yields the plate solution for a given image describing the mapping between our camera frame on the sky and a topocentric celestial angular coordinate frame (right ascension and declination). With the plate solution completed, the image goes through a more detailed conditioning and centroid extraction process to provide not only the pixel locations, but celestial coordinates of light sources in the image. A precession correction using the FK5 system is applied to these coordinates so that they are expressed in the J2000 frame.

With a direct mapping between camera frame and J2000 celestial coordinates, along with very precise centroid information, the next step is to compute the photon flux for each point source in the image. Since our observation cadence is to track on the desired object, stars will inevitably be slightly streaked. To account for this, we use an elliptical aperture method to calculate flux. We estimate the desired aperture to be 2.5 times larger than the FWHM of the average point source PSF in a given frame. The ZWO cameras we use have tunable gain in centibels and is straightforward to calculate the approximate e^-/ADU shown in Eq. 4.

$$\varphi_i = \sum_{\delta} \sqrt{10^{(1.39-\frac{G}{100})}} * c_{\delta j} \tag{4}$$

In Eq. (4) φ_i represents the total flux of the ith point source. The summation is over some elliptical region δ where $c_{\delta j}$ are the individual pixel ADU counts within that region. Finally, G is the camera gain setting in centibels.

Using the calculated flux of each point source in a given image, the apparent magnitude of that point source can be calculated by Eq. (5).

$$M_i = -2.5log_{10}\left(\frac{\varphi_i}{t}\right) + M_0 \tag{5}$$

Here M_i is the calculated apparent magnitude and $M_0$is the zero-point offset for this approximation that is calculated separately and depends largely on the filter used.

5. DATA ANALYSIS

To illustrate the photometric differences of RSOs across multiple filters we have observed both active and inactive (tumbling) targets at different altitudes in LEO, as well as four Geostationary satellites. For brevity only 3 LEO RSOs will be discussed, and for ease of reference they will be referred to as Object (1,2,3). The appropriate catalog ID is known for only two of these satellites and the information about all the satellites discussed in this paper is available in Table 3 below. The four Geostationary satellites were the "cluster" of ANIK F1, ANIK F1R, ANIK G1, and ECHOSTAR 17, which all fit well within the field of view of our telescopes at once. Representations of each of the four GEO satellites can be found in Fig. 2.

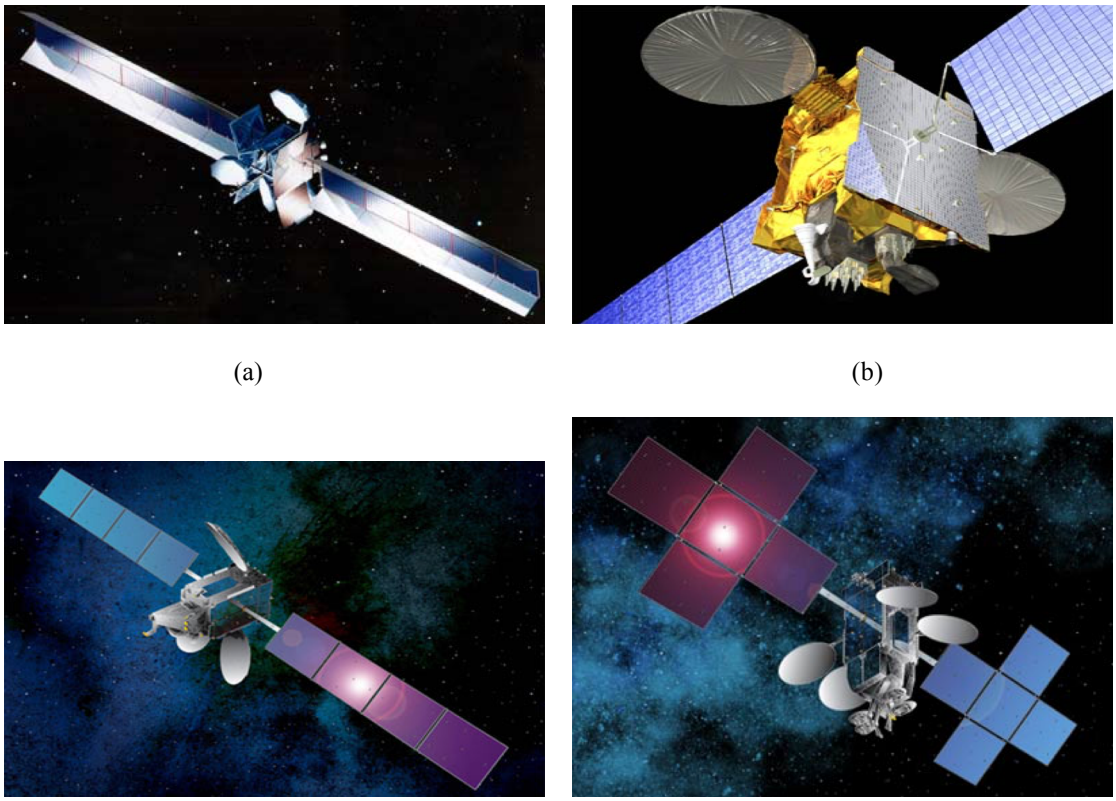

(a) (b)

(c) (d)

Fig. 2. These are representations of the four Geostationary satellites ANIK F1 (a), ANIK F1R (b), ANIK G1 (c), ECHOSTAR 17 (d).

The four Geostationary satellites were observed for an entire night using the Leo-20 telescope. Since Leo-20 is only a single aperture, subsequent exposures switched back and forth between a Sloan g' and z' filter for the entire night. While not technically simultaneous photometry, looking at the light curves produced from each filter over the course of the night still gives insight into how these objects differ in the respective wavebands, and even offers easy visual disambiguation between the three ANIK satellites, which can be notoriously difficult to tell apart. Fig. 3-6 has plots of a single night of observations of all four satellites.

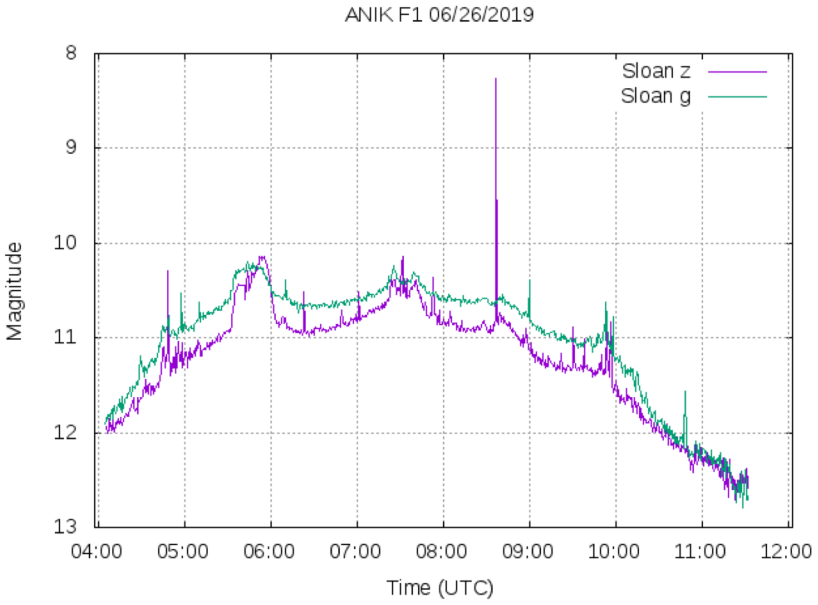

Fig. 3. Nightly light curve of ANIK F1 over the night of 6/26/2019 as seen from Tucson, AZ, in Sloan z and g filters.

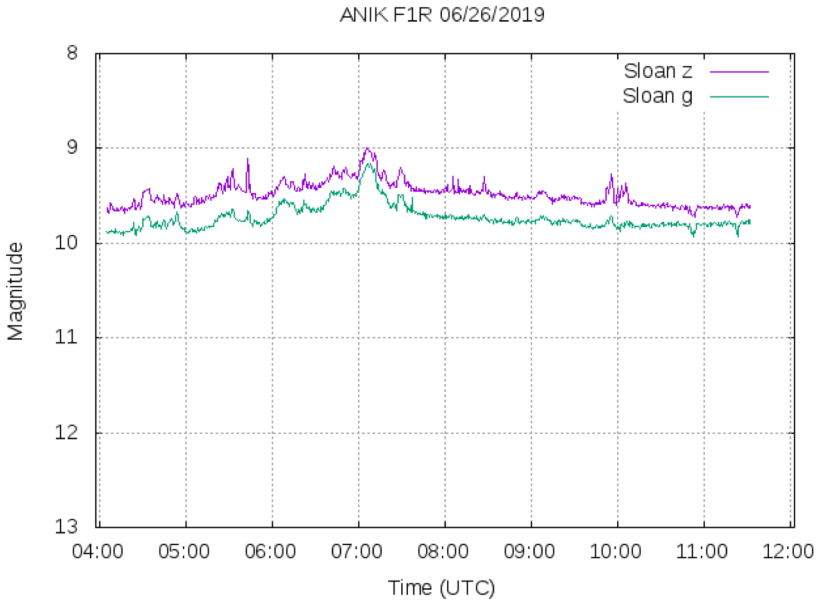

Fig. 4. Nightly light curve of ANIK F1R over the night of 6/26/2019 as seen from Tucson, AZ, in Sloan z and g filters.

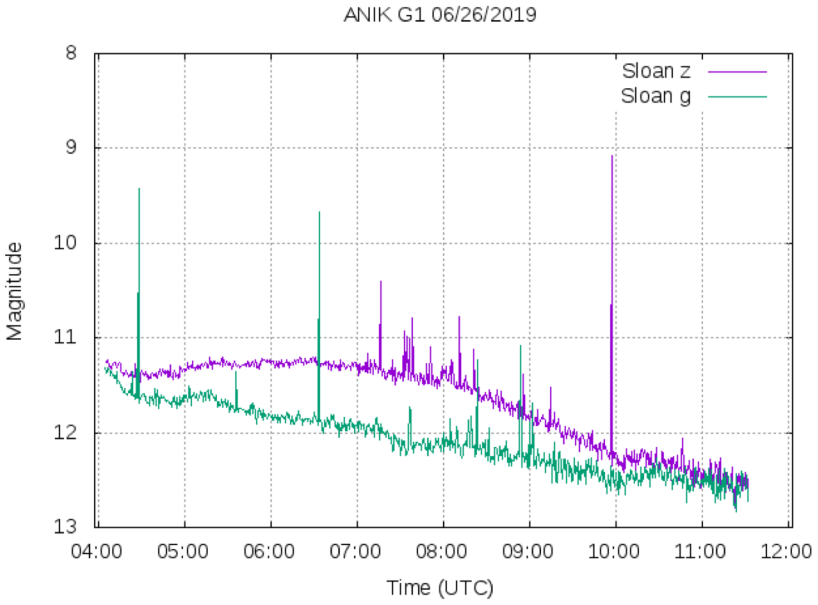

Fig. 5. Nightly light curve of ANIK G1 over the night of 6/26/2019 as seen from Tucson, AZ, in Sloan z and g filters.

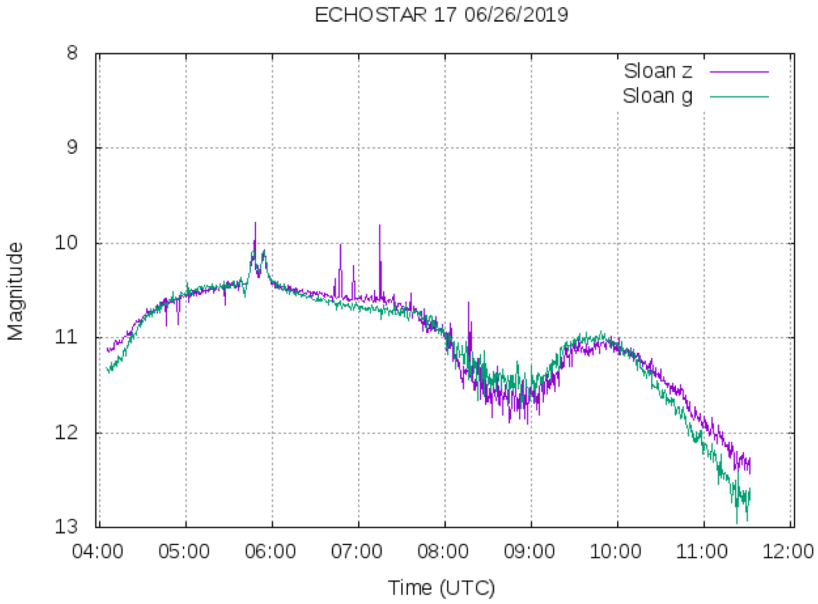

Fig. 6. Nightly light curve of ECHOSTAR 17 over the night of 6/26/2019 as seen from Tucson, AZ, in Sloan z and g filters.

It is encouraging to see that these four different satellites have very different photometric signatures. Moreover, seeing that the two satellites with the most similar construction (ANIK F1R and ANIK G1) share curves that while distinct, have a similar level trend, especially when compared to the other two satellites. The less modest shapes of ANIK F1 and ECHOSTAR 17 are apparent in the light curves where their more complex features give rise to a more

feature-rich result. The high-frequency "instantaneous" spikes in the data are a result of stars passing near/through the aperture used to calculate the flux of each object.

Table 3. General information about the satellites observed.

Name	Catalog ID (NORAD)	Orbit Altitude (km)
ANIK F1	26624	35,780
ANIK F1R	28868	35,788
ANIK G1	39127	35,787
ECHOSTAR 17	38551	35,785
Object 1 (COSMOS …)	-	-
Object 2 (GLOBALSTAR M091)	37741	1,420
Object 3 (LEMUR 2)	41873	500

After these results from the data collected with Leo-20, we proceeded to collect the observations of the LEO objects. All data of the LEO objects was collected from a single pass of each object using the MOA telescope. With this telescope, all four "colors" were collected simultaneously. After some trial observations, we found that the cameras were not sensitive enough in the Sloan u' band so we elected to use that camera unfiltered to compare to the other results.

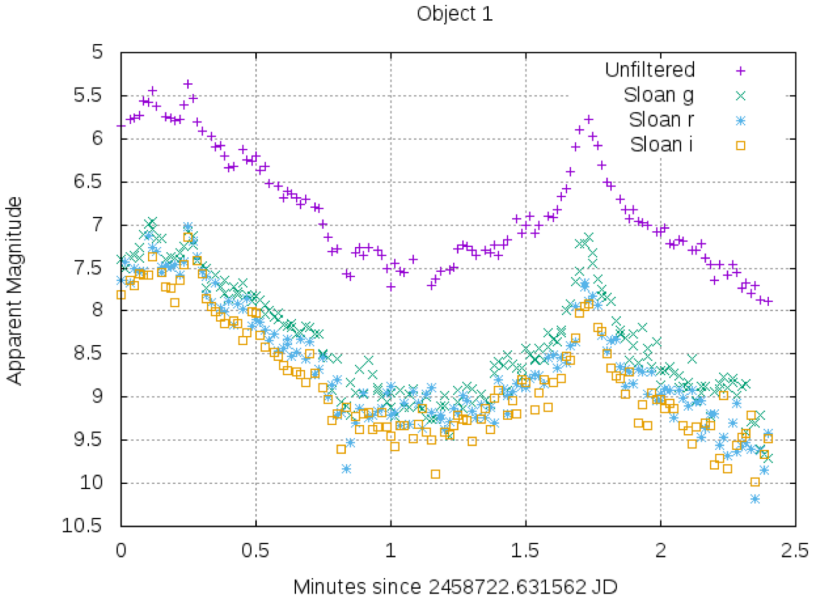

Fig. 7. Photometric light curves of COSMOS objects as it passed over Tucson, AZ on 8/27/2019 in four band passes.

Unfortunately, while collecting the data for Object 1, the actual satellite ID was misplaced so all that is known is that it is one of the COSMOS objects. From the light curve, we can see that this object was rotating with a period of approximately 1.5 minutes.

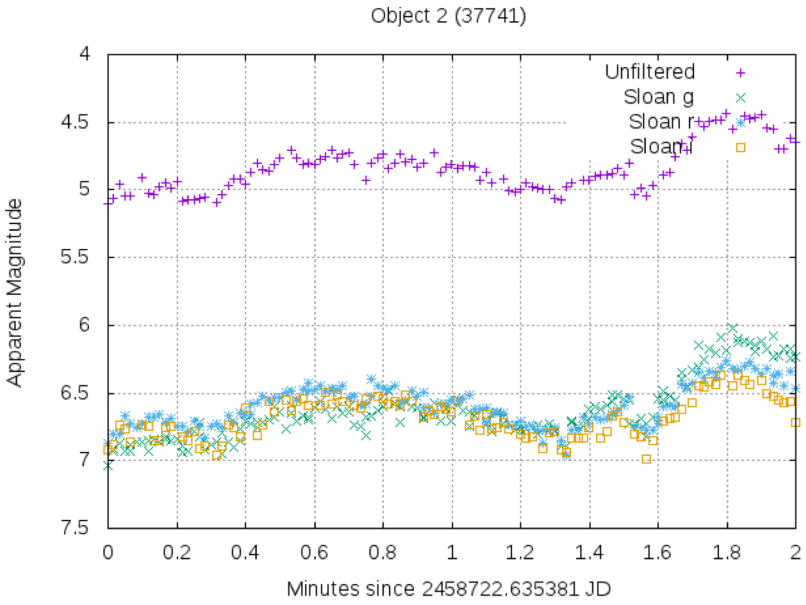

Fig. 8. Photometric light curve of GLOBALSTAR M091 as it passed over Tucson, AZ on 8/27/2019 in four band passes.

Object 2 is a GLOBALSTAR communication satellite, and as such is stabilized which is obvious from the light curve when compared to the rotating Object 1. There still appears to be small oscillations about the stabilization with a period of approximately 1 minute.

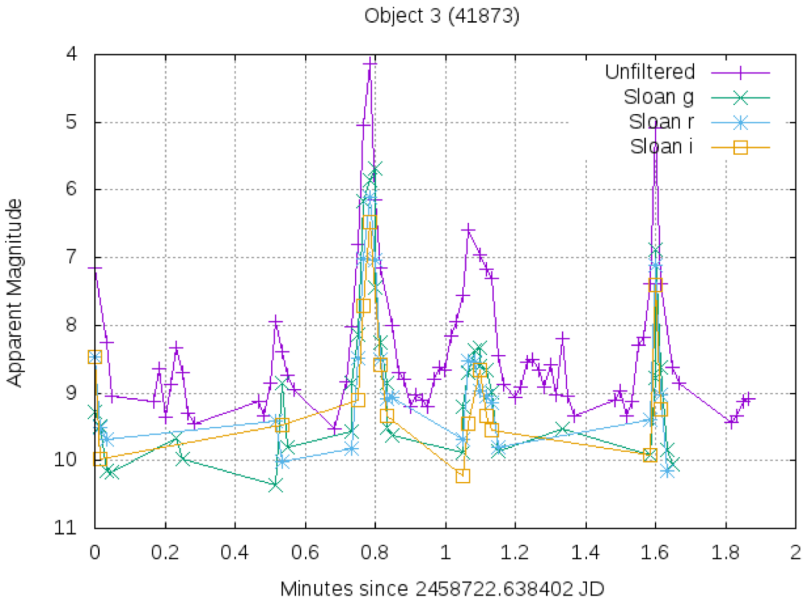

Fig. 9. Photometric light curve of LEMUR 2 ANUBHAVTHAKUR as it passed over Tucson, AZ on 8/27/2019 in four band passes. The lines were added to help with the sparsity of the data as the object was tumbling and flashing in and out of view.

Lastly Object 3 is a 3U Cubesat part of the LEMUR 2 constellation used for ship traffic tracking and meteorology. This particular Cubesat was tumbling during its pass overhead, and as a result would periodically dip below an apparent magnitude of 10 so it would be too dim to be picked up by MOA. Lines have been added through the data points in Fig. 9 to make the periodicity of the data more easily visible.

6. CONCLUSIONS AND FUTURE WORK

We have demonstrated that multi-color simultaneous photometric measurements have tremendous potential for RSO characterization. Observing the RSO in discrete wavelength bands simultaneously at a high frame rate offers multiple independent channels of data that can be used to infer details about the RSO's behavior, shape, and composition. As noted earlier, our primary focus has been to experiment with this technology and develop methods that allow us to build up a database of RSO characterization information. The next step is to further improve the photometric process. Our method of using solar type stars in each image to calibrate our photometry seems to work well for Geostationary satellites where your airmass is relatively unchanged throughout the night, and you have deeper scans (longer exposure time). We did, however, run into trouble with this method when observing objects in LEO. The rapid horizon-to-horizon field of regard coupled with the very short exposures means that there is not always an abundance of solar type stars for calibration use, especially with the filters in the wavelengths where the cameras are less sensitive. We may need to take a more classical approach by observing standard calibration stars before observing such fast moving targets.

7. ACKNOWLEDGMENTS

This work is supported by the Arizona Board of Regents Innovation Fund (PI: Prof. Vishnu Reddy) and the State of Arizona Technology and Research Initiative Fund (PI: Prof. Vishnu Reddy).

This work has made use of data from the European Space Agency (ESA) mission Gaia (https://www.cosmos.esa.int/gaia), processed by the Gaia Data Processing and Analysis Consortium (DPAC, https://www.cosmos.esa.int/web/gaia/dpac/consortium). Funding for the DPAC has been provided by national institutions, in particular the institutions participating in the Gaia Multilateral Agreement.

This work has made use of CyVerse which is supported by the National Science Foundation under Award Numbers DBI-0735191, DBI-1265383, and DBI-1743442. URL: www.cyverse.org

8. REFERENCES

1. T. Campbell, V. Reddy, J. Larsen, R. Linares, R. Furfaro, "Optical Tracking of Artificial Earth Satellites with COTS Sensors," AMOS Technologies Conference, Maui Economic Development Board, Kihei, Maui, HI, Sept. 2018.

2. V. Reddy, T. Linder, R. Linares, R. Furfaro, S. Tucker, T. Campbell, "RAPTORS: Hyperspectral Survey of the GEO Belt," AMOS Technologies Conference, Maui Economic Development Board, Kihei, Maui, HI, Sept. 2018.

3. E. Pearce, A. Ford, T. Schildknecht, V. Reddy, A. Block, K. Rockowitz, "Rapid Characterization of Geosynchronous Space Debris with 5-color Near-IR Photometry," AMOS Technologies Conference, Maui Economic Development Board, Kihei, Maui, HI, Sept. 2017.

4. E. Cordelli, P. Schlatter, T. Schildknecht, "Simultaneous multi-filter photometric characterization of space debris at the Swiss Optical Ground Station and Geodynamics Observatory Zimmerwald," AMOS Technologies Conference, Maui Economic Development Board, Kihei, Maui, HI, Sept. 2018.

5. D. Vallado. *Fundamentals of Astrodynamics and Applications*. Microcosm Press, Hawthorne, CA, Fourth Edition, 2013.

6. Finger Lakes Instrumentation, "ProLine PL 16803," PL16803 datasheet, 2018.

7. Finger Lakes Instrumentation, "ProLine PL 4710 DD," PL4710DD datasheet, 2018.

8. ZWO, "ASI1600MM Pro", ASI datasheet, 2019.

9. Sidereal Technology, "SiTech Time Server Manual," SiTech Time Server datasheet, 2018.

10. Gaia Collaboration et al. (2016): Description of the Gaia mission (spacecraft, instruments, survey and measurement principles, and operations).

11. Gaia Collaboration et al. (2018b): Summary of the contents and survey properties.